Measurement of minority carrier diffusion lengths in GaAs nanowires by a nanoprobe technique

A. Darbandi and S. P. Watkins[a)]
Department of Physics, Simon Fraser University, Burnaby, British Columbia V5A 1S6, Canada

(Received 14 March 2016; accepted 21 June 2016; published online 1 July 2016)

Minority carrier diffusion lengths in both p-type and n-type GaAs nanowires were studied using electron beam induced current by means of a nanoprobe technique without lithographic processing. The diffusion lengths were determined for Au/GaAs rectifying junctions as well as axial p-n junctions. By incorporating a thin lattice-matched InGaP passivating shell, a 2-fold enhancement in the minority carrier diffusion lengths and one order of magnitude reduction in the surface recombination velocity were achieved. *Published by AIP Publishing.*
[http://dx.doi.org/10.1063/1.4955136]

I. INTRODUCTION

Semiconductor nanowires (NW) with axial and core-shell structures have been proposed for several optoelectronic applications including light emitting diodes,[1] lasers,[2] and field effect transistors.[3] Recently, an axial GaAs p-n junction nanowire array has shown a photovoltaic conversion efficiency of 15%.[4] Critical factors limiting commercial integration of these devices include the measurement of NW electrical transport characteristics, dopant distributions, contact junction properties, and surface state densities. Due to the large surface-to-volume ratio in NWs, the sidewall surface states play a major role in governing the electronic properties of NW devices.[5] Surface states result in the reduction of the minority carrier diffusion length (L_d) in semiconductor NWs due to their role as recombination centers.[6] L_d ranges between 0.1 and 10 μm in bulk GaAs[7] depending on the doping concentration and surface recombination velocity. If L_d is shorter than the NW geometrical length, the minority carriers recombine before diffusing to the junction. Therefore, understanding of the minority carrier transport and improvement of L_d are important goals in designing NW based devices.

Minority carrier diffusion lengths can be measured by several techniques. Photo-current microscopy with a scanning laser beam has been used to study PbS and Si NWs.[8,9] It was found that the hole diffusion length in Si varies within a range of 25 nm–2 μm for a diameter dispersion of 30 nm–900 nm. The observed upper limit approaches the behavior of bulk silicon. Low temperature cathodoluminescence of GaAs/AlGaAs NWs at 7 K (Ref. 10) resulted in $L_d = 0.15 \pm 0.04$ μm for intrinsic GaAs. Recently, electron beam induced current (EBIC) measurements of unpassivated GaAs NWs have also been carried out which suggested an average L_d of 0.1 ± 0.05 μm (Ref. 11) for NWs with 100–300 nm diameter range. Previous literature[8–11] used extensive chemical lithography processing for contact deposition or required cryogenic conditions. In this work, we report a technique to investigate room temperature EBIC using *in situ* nanoprobe measurements with no lithographic processing. This was done inside a scanning electron microscope (SEM), which enables us to readily analyze an ensemble of NWs without removing them from the substrate. Measurements were performed on Schottky NW devices as well as axial p-n structures. A lattice matched InGaP passivation shell was found to significantly reduce the surface recombination velocity of these devices.

II. EXPERIMENT

Fig. 1 shows the experimental setup of our EBIC measurements. The tip of each free-standing NW is contacted with a tungsten nanoprobe inside a SEM, while the substrate serves as the bottom contact.[12] The substrate is grounded via the SEM stage and the nanoprobe voltage is applied by a Keithley 4200 source-measurement unit (SMU). The SMU sweeps the voltage with steps of 50 μV and the current is measured simultaneously with a 30 pA accuracy. Sample preparation was minimal and only required the cleaving of the substrate and mounting on 45° oriented Al stubs. Indium was used on the back side of the substrate to ensure electrical contact to the stub, and the stage was rotated manually to achieve 90° orientation of the beam with respect to the NW axis. For the EBIC measurements, an e-beam of 5 kV accelerating voltage was used. The e-beam current was 3 pA with a 20 nm spot size. These beam parameters were chosen to ensure low excitation conditions in the NWs used in this study. Beam focus was established by imaging and EBIC scans were performed in line-scan mode using the same beam conditions used for imaging. We carried out EBIC at zero bias with 1 s dwell time per point.

Three types of structures were fabricated as indicated in Fig. 1. In the first structure, single carrier n-type NWs were grown on an n-type substrate. The depletion region under the Au catalyst particle was used to collect minority carriers (Fig. 1(a)). In the second structure, p+n$^+$ axial homojunction NWs structures were grown and the EBIC signal was measured separately on either side of the NW junction. The Au nanoparticle (NP) forms an ohmic contact[5] due to the heavy p-doping (Fig. 1(b)). In the third structure, a p-type GaAs

[a)]Electronic mail: simonw@sfu.ca

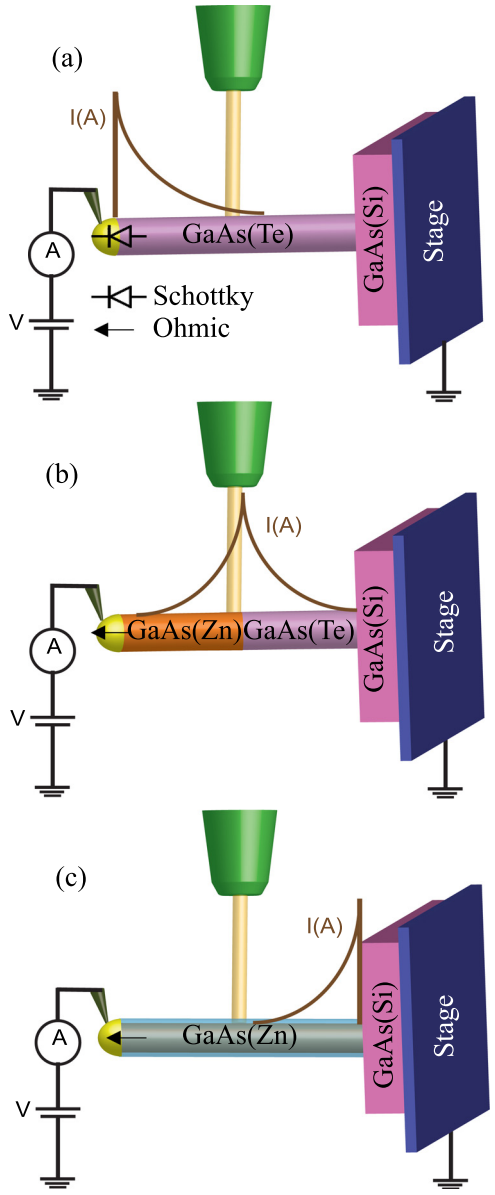

FIG. 1. Schematic of EBIC measurements performed with *in situ* nanoprobe technique inside SEM: (a) Schottky junction n-type GaAs NW on n-type substrate, (b) axial homostructure GaAs p-n junction NW with ohmic terminals, and (c) passivated p-type GaAs/InGaP NW on a n-type substrate. Expected EBIC signal as a function of position is indicated schematically above each structure.

core was grown on an n-type GaAs substrate, placing the junction at the substrate/NW boundary (Fig. 1(c)). The third structure was used to reveal the effect of surface passivation on the diffusion lengths of the p-type GaAs cores, by a thin shell of lattice matched InGaP. This structure eliminates complications arising from InGaP passivation for the other two structures. Specifically for structure (a), InGaP passivation results in the growth of an unwanted neck region, while in (b), a p-doped shell will have unwanted effects on the n-doped segment. The n-type passivation of GaAs(Te) NWs was also carried out using a 20 nm thick n-type GaP shell on the structure indicated in Fig. 1(a).

Growth of GaAs NWs begins by depositing a thin gold layer of 4 nm on (111)B Si-doped (3×10^{18} cm^{-3}) GaAs substrates using vacuum evaporation deposition. We formed Au nanoparticles (NPs) by annealing the substrate at 450 °C for 1 min under H_2 and tertiarybutylarsine (TBAs) overpressure in a metalorganic vapor phase epitaxy (MOVPE) reactor. The group III and V precursors were trimethylgallium (TMGa) and TBAs, respectively. TMGa and TBAs flow rates were set to 17 and 160 μmol/s to grow GaAs NWs at 400 °C. Te-doping was carried out by introducing H_2-diluted diethyltellurium (DETe) during the growth with a molar flow of 0.05 μmol/min. A representative SEM image of this sample is shown in Fig. 2(a). A p-type GaAs NW structure (unpassivated sample of Fig. 1(c)) was grown using similar TMGa and TBAs molar flows, and diethylzinc (DEZn) as the p-type precursor with a flow rate of 0.04 μmol/min.

The axial p-n structure of Fig. 1(b) was also grown using the same growth conditions as stated before by promptly switching from DETe to DeZn with no growth interrupt. The corresponding SEM image of this sample is shown in Fig. 2(b) where the device is contacted by the nanoprobe at the Au NP. The secondary electron intensity is higher from the top p-type GaAs(Zn) segment compared to the bottom n-type GaAs(Te) region. This higher secondary electron emission intensity in p-type GaAs(Zn) is due to the lowered surface barrier compared to n-type GaAs(Te).[13,14]

Surface passivation of GaAs NWs was investigated by two methods, both using the structure shown in Fig. 1(c). A 15 nm InGaP(Zn) passivating shell was grown on an array of p-type cores at 450 °C using triethylgallium (TEGa), trimethylindium (TMIn), tertiarybutylphosphine (TBP), and DEZn as the III, V, and p-type doping precursors, with molar flows of 9.7 μmol/min, 7.3 μmol/min, 0.96 mmol/min, and 0.4 μmol/min, respectively. Lattice matching conditions for InGaP on GaAs were obtained by growth of thin films on GaAs (001) substrates. Passivation of n-type GaAs(Te) NWs using a 20 nm thick GaP shell was also investigated using growth conditions similar to those stated earlier.

III. RESULTS AND DISCUSSION

Figure 2(a) shows a representative image of the cleaved edge of a typical GaAs NW array oriented perpendicular to the electron beam, appropriate for EBIC measurements. Figure 2(b) shows a detail of the W nanoprobe contacting a Au nanoparticle on the end of a p-n junction. The p-type side of the junction is closest to the Au NP and shows enhanced secondary emission due to the enhancement of the surface electric field for p-type surfaces due to surface Fermi level pinning.[14] The p-n junction is located 850 nm below the Au NP with a depletion region width of $\sim 80 \pm 10$ nm based on the estimated n- and p-doping levels.

Figure 2(c) shows a representative bright field (BF) transmission electron microscope (TEM) image of the core/shell GaAs/InGaP NW. A 140 nm long InGaP neck is seen at the tip of the NW. Image contrast around the InGaP neck is the result of stacking faults formed while ramping the reactor temperature to 450 °C for InGaP growth. The observed image contrast at the edges of the NW is due to Fresnel fringes. High resolution TEM lattice imaging (not shown) confirmed a condition close to lattice matched with no edge dislocations. GaP shells with comparable thickness of

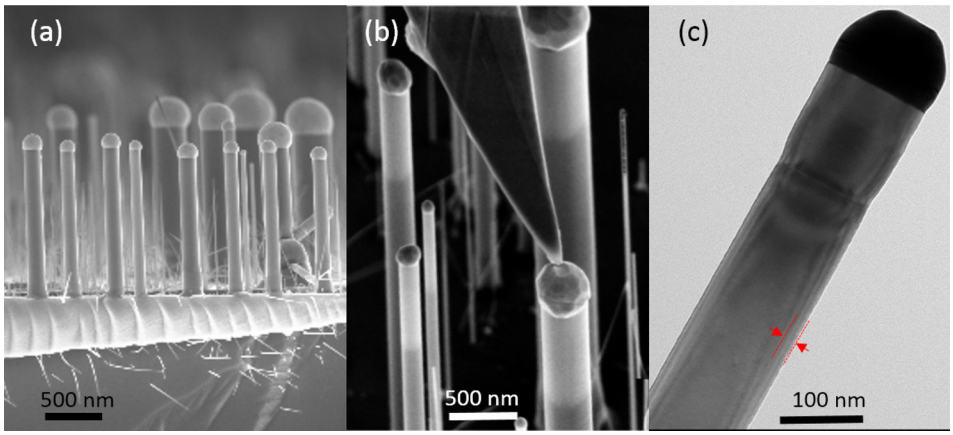

FIG. 2. SEM images of (a) as-grown GaAs(Te) NWs, and (b) axial GaAs p-n junction NW without surface treatment. The nanoprobe contact is shown. (c) BF-TEM image of a GaAs NW with 15 nm lattice matched InGaP passivating shell. Arrows indicate the location of the InGaP shell.

~20 nm (not shown) were observed to have clearly visible defect structure.

The electrical properties of axial GaAs p-n NWs were examined using a nanoprobe inside the SEM. The nanoprobe is connected directly to the Au NP which forms an Ohmic contact with the highly Zn doped p-type end of the NW. Fig. 3(a) shows the measured J-V characteristics of several NWs with various diameters. The p-n diode behavior was observed with over six decades of current rectification. The NW series resistance dominates the conduction at voltages above 1.5 V. Analysis of the slope of the forward bias currents gives an average diode ideality factor of 2.1 which indicates a recombination controlled process at the junction. The carrier concentration of each p-type and n-type segment was evaluated through two separate growths where only single carrier type NWs were grown. Nanoprobe measurements resulted in estimates of the n-type and p-type concentrations of $4\pm1\times10^{17}\,\mathrm{cm}^{-3}$ and $3\pm1\times10^{19}\,\mathrm{cm}^{-3}$, respectively, based on resistivity vs. concentration data for uncompensated GaAs.[15]

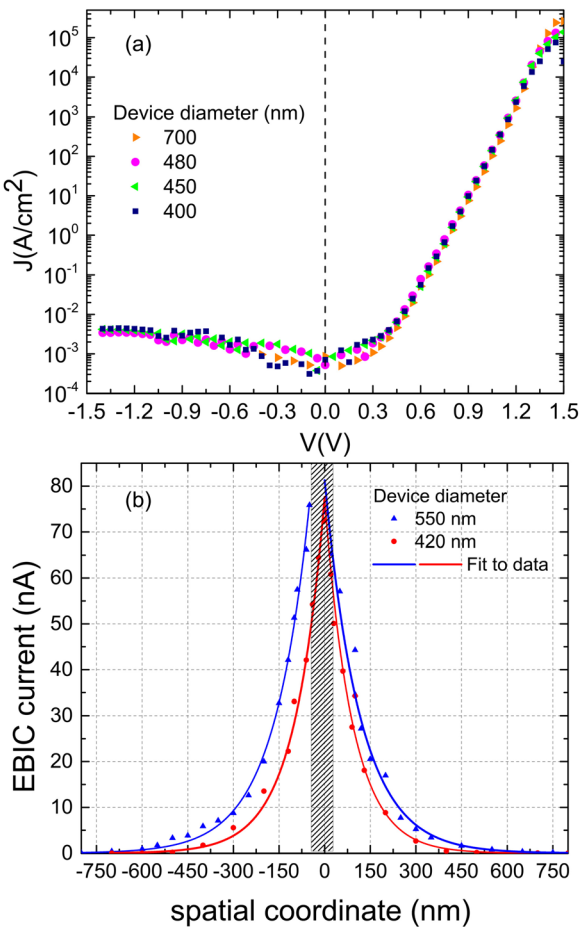

FIG. 3. (a) Current-voltage properties of several representative axial GaAs p-n devices and (b) measured EBIC current for representative axial GaAs p-n devices. The solid line shows the exponential decay fit to the experimental data to extract the carrier diffusion length.

In order to obtain accurate estimates of the minority carrier diffusion lengths, the low level injection condition must be satisfied. This means that the excess minority carrier concentration δp must be less than the majority electron concentration, n_0. The excess carrier generation rate, G, can be estimated by Davidson's equation which contains the product of the beam current and the beam voltage as $G \propto \frac{I_b V_b}{qE_i}$, where E_i is the e-h pair creation energy and I_b and V_b are the beam current and voltage, respectively.[16] Assuming a spherical volume of interaction for the electrons inside the semiconductor, the excess carrier generation rate per unit volume can then be calculated using the electron range.[17] We estimated $G = 2\times10^{25}\,\mathrm{cm}^{-3}\,\mathrm{s}^{-1}$, and the excess carrier concentration can then be calculated by $\delta p = p_0 + \tau_n G \approx \tau_n G$,[15] which leads to a maximum δp of $5\times10^{14}\,\mathrm{cm}^{-3}$. Therefore, the low level injection condition of $\delta p \ll n_0$ is fulfilled in our measurements.

The measured EBIC currents of two representative axial p-n GaAs NWs are shown in Fig. 3(b) as a function of axial displacement along the NW. The zero reference position in the figure marks the location of the p-n junction with the dashed area indicating the depletion region width. The negative value displacements correspond to the p-type segment, while the positive values correspond to the n-type GaAs segment. The EBIC decays exponentially from a maximum value of 75 nm at the junction to 5 pA in the neutral region. The diffusion lengths of the minority carriers were obtained by fitting the experimental data to the following expression:

$$I = I_0 \exp^{-d/L_i}, \tag{1}$$

where I_0 is the maximum EBIC intensity, d is the beam displacement from the junction, and L_i is the diffusion length in the p- or n-type semiconductor. The solid lines in Fig. 3(b)

show this theoretical fit. The extracted maximum diffusion lengths for holes and electrons are 116 ± 5 nm and 119 ± 4 nm, respectively. In order to understand the effect of the junction type on the collected minority carriers, we performed EBIC measurements on single carrier GaAs(Te) NWs using the electric field under the Au contact depletion region to collect the carriers (Fig. 1(a)). The measured hole diffusion lengths with respect to NW diameters are shown in Fig. 4(a) for both Schottky and p-n junction structures. Several devices with diameters in the range of 100 nm–550 nm were examined and a diameter dependent hole diffusion length was observed between 60 nm and 120 nm. Results agree well with those obtained from p-n junction devices (blue markers). The obtained diffusion lengths are consistent with the values reported for Sn doped GaAs NWs (100 ± 30 nm).[11] However, these are still lower than the bulk and thin film GaAs L_d values by about a factor of 10.[18,19]

Hole lifetimes can be calculated by the Einstein equation $L_n = \sqrt{D_n \times \tau_n}$, where D_n is the carrier diffusion coefficient in n-type GaAs. Assuming D_n of 5.2 cm^2/s in GaAs with a concentration of $n = 4 \pm 1 \times 10^{17}$,[7] the calculated hole lifetime, τ_n, is 7–25 ps depending on the NW diameter. The reported lifetime in bulk GaAs with the same doping level is 50 ns which is larger than the NW results by at least 3 orders of magnitude.[7]

The τ_n dependence on NW diameter is attributed to surface states at the GaAs NW sidewalls which act as recombination sites. Neglecting bulk recombination, the effective carrier lifetime of a semiconducting cylinder with surface recombination can be obtained by solving the continuity equation for the excess carrier concentration $\delta n(r,t)$

$$\frac{\partial \delta n(t,r)}{\partial t} = D \frac{1}{R} \frac{\partial}{\partial r} \left(r \frac{\partial \delta n}{\partial R} \right), \tag{2}$$

where D is the diffusion coefficient. The boundary condition at the surface of a semiconducting cylinder with radius a is given by

$$D \frac{\partial \delta n(r,t)}{\partial r} = -Sn(r,t) \qquad \text{for } r = a, \tag{3}$$

where S is the surface recombination velocity. The continuity equation can be solved analytically,[20] which leads to the carrier concentration decaying exponentially at the surface with a time constant of $a^2/\beta^2 D$.[21] In the presence of both bulk and surface recombination, an effective carrier lifetime can be estimated as[21]

$$\frac{1}{\tau_{eff}} = \frac{1}{\tau_0} + \frac{\beta^2 D}{a^2}, \tag{4}$$

where β is given by the solution of

$$\beta J_1(\beta) - (aS/D) J_0(\beta) = 0. \tag{5}$$

J_0 and J_1 are Bessel functions of the first kind. We extract the surface recombination velocity by fitting the experimental L_d data using Eqs. (4) and (5) as shown by the black solid line in Fig. 4(a). This leads to $S = 4.7 \pm 0.1 \times 10^5$ cm/s in our n-type GaAs(Te) NWs which is comparable to a reported bulk value of $3 \pm 1 \times 10^5$ cm/s (Ref. 22) for GaAs(Te) with $n = 1 \times 10^{17}$ cm^{-3}.

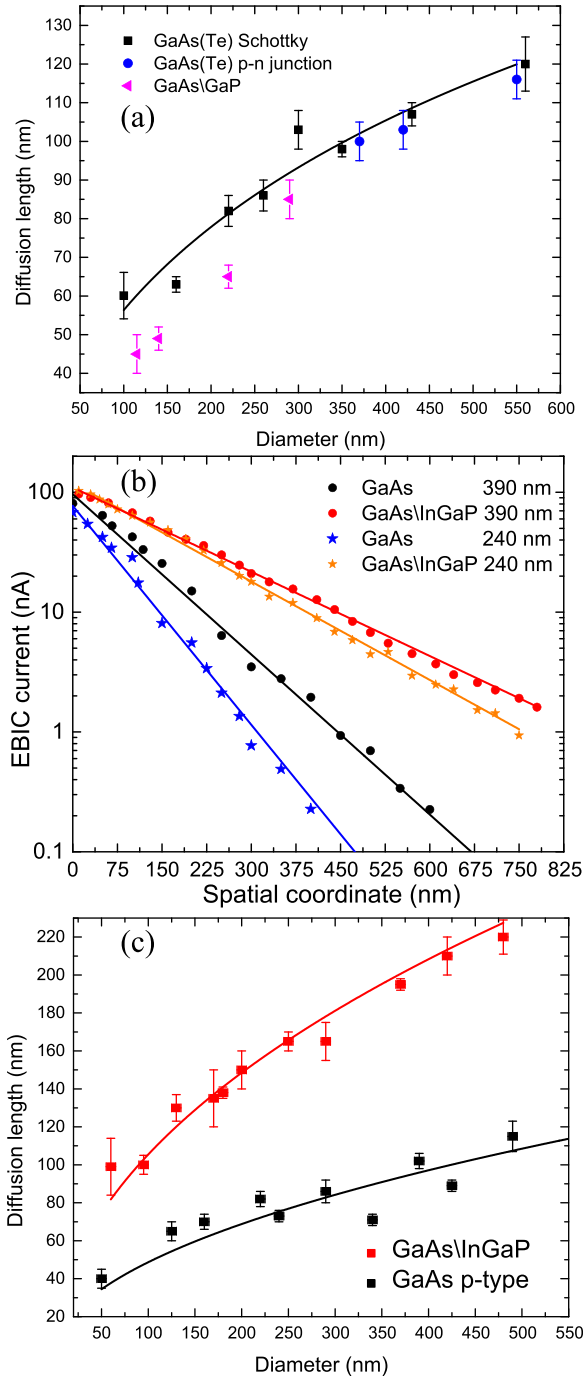

FIG. 4. (a) Hole diffusion lengths, measured with Schottky and p-n junction methods, with respect to NW diameters. The effect of the GaP shell passivation on the minority carrier diffusion length is also shown. The solid line is a fit to the experimental data. (b) EBIC of a few representative lattice matched GaAs/InGaP NWs compared to unpassivated p-type GaAs NWs. (c) Electron diffusion lengths in p-type GaAs NWs measured before and after InGaP passivation for various NW diameters.

Previously reported diffusion lengths in semiconductor NWs fall below those of the corresponding bulk counterparts by at least an order of magnitude.[8–11,23] This significant reduction is attributed to the high number of surface states in

NWs. EBIC studies of surface passivated GaAs NWs with aqueous ammonium sulfide resulted in a small improvement of 20% in L_d.[11] The poor stability of the latter passivation lasted less than 96 h and it introduced even more surface defects which eventually reduced the minority carrier L_d values below that of the original unpassivated NWs. In order to investigate the effect of surface treatment on the recombination velocity, EBIC measurements were carried out on the GaAs/GaP core-shell NWs. Representative data from several devices are shown in Fig. 4(a). It was observed that the thick relaxed GaP shell was ineffective in passivating the surface. We might assume each dislocation is a line of point defects that wraps around the core NW. Given the GaAs lattice constant a, one can then estimate an interface defect density of $\rho \approx 2/aD_e = 1.2\pm0.2 \times 10^{13}$ cm^{-2} which is comparable to the reported bulk GaAs surface states density of $3\pm1 \times 10^{13}$ cm^{-2}.[24] In other words, the GaAs surface states have been replaced by another set of states (dislocations) so that no improvement in transport properties is observable.

A better surface treatment of GaAs NWs can be achieved by AlGaAs or lattice matched InGaP passivation. Self catalyzed AlGaAs/GaAs NWs showed a 6-fold improvement in the EBIC measured minority carrier diffusion lengths of core GaAs;[25] however, the unpassivated L_d value was extremely low (30 nm). Low temperature PL measurements of InGaP passivated undoped InGaAs NWs have shown a factor of 5 improvement in carrier lifetime.[26] Au-assisted GaAs/$In_{0.52}Ga_{0.48}P$ NWs also showed a 2 order of magnitude enhancement in the PL intensity of core GaAs NWs at 5 K.[27] In this work, we directly measure the diffusion lengths of GaAs/InGaP core-shell nanowires at room temperature. EBIC measurements of p-type GaAs(Zn) NWs with and without InGaP shells were carried out using the structure illustrated in Fig. 1(c). Representative EBIC measurements as a function of axial displacement from the junction are shown in Fig. 4(b) for several devices with various diameters. EBIC signals with a maximum of 100 nA were obtained near the junction, and decayed exponentially over a range of less than 900 nm. It can be seen that the decay currents of GaAs/InGaP NWs have a lower slope than those of unpassivated GaAs NWs confirming an improvement in the diffusion length. The solid lines represent the linear fit to the experimental data to extract the electron diffusion lengths. The results are shown in Fig. 4(c) for NW diameters in the range of 50 nm–500 nm. Similar to the n-type GaAs NWs, a diameter dependent L_d was observed which varied from 40 nm to 220 nm. These values are lower than those reported for bulk p-type GaAs by an order of magnitude.[19,28] A 2-fold enhancement in the electron diffusion lengths was obtained by InGaP passivation. The corresponding electron lifetimes, τ_p, were then calculated using the Einstein equation with $D_p = 26$ cm^2/s (Ref. 7) (for $N_A \sim 10^{19}$ cm^{-3} at 300 K). In unpassivated GaAs, τ_p varies between 0.6 ps and 4 ps, while the electron lifetime increases by an average factor of 5 in InGaP passivated NWs. The results are summarized in Table I for both electrons and holes in GaAs NWs and also the InGaP passivated p-type GaAs NWs. The solid lines in Fig. 4(c) show the theoretical fit using the method stated earlier to extract the surface recombination velocity. The

TABLE I. Minority carrier diffusion lengths, L_d, lifetime, τ, and surface recombination velocity, S, in n-type GaAs, p-type GaAs, and GaAs/InGaP NWs.

Sample	Doping (cm^{-3})	L_d (nm)	τ (ps)	S (cm/s)
GaAs	Te: 4×10^{17}	60–120	7–25	$4.7\pm0.1 \times 10^5$
GaAs	Zn: 3×10^{19}	40–110	0.6–4	$3.0\pm0.3 \times 10^6$
GaAs/InGaP	Zn: 3×10^{19}	100–220	4.1–18.6	$5.5\pm0.5 \times 10^5$

GaAs(Zn) NWs exhibit a recombination velocity of $S_p = 3 \pm 0.3 \times 10^6$ cm/s which is comparable to that of bulk GaAs with $S_p = 3\pm1 \times 10^6$ cm/s (Ref. 22) (for $N_A \approx 10^{19}$ cm^{-3}). The surface recombination velocity is further decreased by an order of magnitude to $S_p = 5.5\pm0.5 \times 10^5$ cm/s for GaAs/InGaP NWs indicating that InGaP passivation is a promising route to reduce surface recombination in GaAs NWs.

Finally, the EBIC data can be used to directly estimate the injected excess carrier concentration from simple diffusion current arguments. The hole diffusion current density in an n-type semiconductor is $J_p(x) = -eD\frac{dp(x)}{dx}$ with $p(x) = \delta p e^{-\frac{x}{L}}$, where D and L are the minority carrier diffusivity and diffusion length, respectively. By evaluating the derivative and using the experimental L and the measured $J_p(0)$ for the boundary conditions, we obtained a mean δp of 5.6×10^{14} cm^{-3} for the unpassivated Au/n-GaAs NW junctions (Fig. 1(a)) which agrees with our previous estimate based on the beam voltage and current, and clearly satisfies the low level injection condition, $\delta p \ll n_0$.

IV. CONCLUSION

In summary, we measured the minority carrier diffusion lengths in both p-type and n-type GaAs nanowires using electron beam induced current (EBIC) by means of a simple lithography-free nanoprobe technique. The measured diffusion lengths were identical in both Schottky and axial p-n junction terminal configurations. An improvement of charge carrier lifetime in GaAs nanowires was obtained by a thin lattice-matched InGaP passivating shell. As a result, a 2-fold enhancement in the electron diffusion lengths and one order of magnitude reduction in the surface recombination velocity were achieved.

ACKNOWLEDGMENTS

The authors gratefully acknowledge funding from the Natural Sciences and Engineering Research Council of Canada. We also acknowledge the support of 4D LABS Nanoimaging staff.

[1]F. Qian, S. Gradecak, Y. Li, C. Wen, and C. M. Lieber, Nano Lett. **5**, 2287 (2005).
[2]B. Hua, J. Motohisa, Y. Kobayashi, S. Hara, and T. Fukui, Nano Lett. **9**, 112 (2009).
[3]W. Fung, L. Chen, and W. Lu, Appl. Phys. Lett. **99**, 092108 (2011).
[4]I. Åberg, G. Vescovi, D. Asoli, U. Naseem, J. P. Gilboy, C. Sundvall, A. Dahlgren, K. E. Svensson, N. Anttu, M. T. Björk, and L. Samuelson, IEEE J. Photovoltaics **6**, 185 (2016).
[5]A. Darbandi, O. Salehzadeh, P. Kuyanov, R. R. LaPierre, and S. P. Watkins, J. Appl. Phys. **115**, 234305 (2014).

[6]H. Ito and T. Ishibashi, Jpn. J. Appl. Phys., Part 1 **33**, 88 (1994).
[7]S. Adachi, *Properties of Group-IV, III-V and II-VI Semiconductors* (John Wiley & Sons, 2005).
[8]R. Graham, C. Miller, E. Oh, and D. Yu, Nano Lett. **11**, 717 (2011).
[9]M. D. Kelzenberg, D. B. Turner-Evans, B. M. Kayes, M. A. Filler, M. C. Putnam, N. S. Lewis, and H. A. Atwater, Nano Lett. **8**, 710 (2008).
[10]J. Bolinsson, K. Mergenthaler, L. Samuelson, and A. Gustafsson, J. Cryst. Growth **315**, 138 (2011).
[11]C. Gutsche, R. Niepelt, M. Gnauck, A. Lysov, W. Prost, C. Ronning, and F. Tegude, Nano Lett. **12**, 1453 (2012).
[12]O. Salehzadeh, M. X. Chen, K. L. Kavanagh, and S. P. Watkins, "Rectifying characteristics of Te-doped GaAs nanowires," Appl. Phys. Lett. **99**, 182102 (2011).
[13]S. Chung, V. Wheeler, R. Myers-Ward, L. O. Nyakiti, C. R. Eddy, D. K. Gaskill, M. Skowronski, and Y. N. Picard, J. Appl. Phys. **110**, 014902 (2011).
[14]I. Volotsenko, M. Molotskii, Z. Barkay, J. Marczewski, P. Grabiec, B. Jaroszewicz, G. Meshulam, E. Grunbaum, and Y. Rosenwaks, J. Appl. Phys. **107**, 014510 (2010).
[15]S. M. Sze and K. K. Ng, *Physics of Semiconductor Devices* (John Wiley & Sons, 2006), p. 7.
[16]S. M. Davidson, J. Microsc. **110**, 177–204 (1977).
[17]T. Everhart and P. Hoff, J. Appl. Phys. **42**, 5837–5846 (1971).
[18]C. J. Hwang, J. Appl. Phys. **40**, 3731 (1969).
[19]H. C. Casey, Jr., B. I. Miller, and E. Pinkas, J. Appl. Phys. **44**, 1281 (1973).
[20]J. Crank, *The Mathematics of Diffusion* (Clarendon, Oxford, 1975).
[21]F. Daiminger, A. Schmidt, F. Faller, and A. Forchel, Proc. SPIE **2139**, 213 (1994).
[22]C. A. Hoffman, H. J. Gerritsen, and A. V. Nurmikko, J. Appl. Phys. **51**, 1603 (1980).
[23]Y. Dan, K. Seo, K. Takei, J. H. Meza, A. Javey, and K. B. Crozier, Nano Lett. **11**, 2527 (2011).
[24]G. S. Chang, W. C. Hwang, Y. C. Wang, Z. P. Yang, and J. S. Hwang, J. Appl. Phys. **86**, 1765 (1999).
[25]C.-C. Chang, C.-Y. Chi, M. Yao, N. Huang, C.-C. Chen, J. Theiss, A. W. Bushmaker, S. LaLumondiere, T.-W. Yeh, M. L. Povinelli, C. Zhou, P. D. Dapkus, and S. B. Cronin, Nano Lett. **12**, 4484 (2012).
[26]H. Sun, F. Ren, K. W. Ng, T.-T. D. Tran, K. Li, and C. J. Chang-Hasnain, ACS Nano **8**, 6833–6839 (2014).
[27]N. Skold, L. S. Karlsson, M. W. Larsson, M.-E. Pistol, W. Seifert, J. Tragardh, and L. Samuelson, Nano Lett. **5**, 1943 (2005).
[28]D. Wight, P. Oliver, T. Prentice, and V. Steward, J. Cryst. Growth **55**, 183 (1981).